

ARTICLE

Open Access

Stretchable multifunctional wearable system for real-time and on-demand thermotherapy of arthritis

Zehan Liu^{1,2}, Xihan Wang^{1,2}, Yiyang He^{1,2}, Weiqiang Hong^{1,2}, Peng Sun^{1,2}, Weitao Liu^{1,2}, Dong Ye³, Zhuoqing Yang⁴, Xuewen Wang⁵, Mengxi Wu^{1,2}✉, Liding Wang^{1,2} and Junshan Liu^{1,2}✉

Abstract

Thermotherapy is a conventional and effective physiotherapy for arthritis. However, the current thermotherapy devices are often bulky and lack real-time temperature feedback and self-adjustment functions. Here, we developed a multifunctional wearable system for real-time thermotherapy of arthritic joints based on a multilayered flexible electronic device consisting of homomorphic hollow thin-film sensors and heater. The kirigami–serpentine thin-film sensors provide stretchability and rapid response to changes in environmental temperature and humidity, and the homomorphic design offers easy de-coupling of dual-modal sensing signals. Based on a closed-loop control, the thin-film Joule heater exhibits rapid and stable temperature regulation capability, with thermal response time < 1 s and maximum deviation < 0.4 °C at 45 °C. Based on the multifunctional wearable system, we developed a series of user-friendly gears and demonstrated programmable on-demand thermotherapy, real-time personal thermal management, thermal dehumidification, and relief of the pain via increasing blood perfusion. Our innovation offers a promising solution for arthritis management and has the potential to benefit the well-being of thousands of patients.

Introduction

Arthritis is a chronic disease that affects the well-being of millions of people all over the world. Featured as the inflammation, swelling, and stiffness around the joints^{1–4}, arthritis brings severe pain and inconvenience to patients, especially the elderly. According to the current consensus of the medical community, arthritis is incurable, while fortunately, it can be relieved by some physical therapies^{5–8}. Among them, thermotherapy can promote local vasodilation, enhance blood perfusion, and thereby alleviate pain and reduce joint stiffness with minimal side effects, thus, it is the most widely used and highly recommended physical therapy to the majority of patients^{9–11}. However, conventional thermotherapy tools (i.e., hot

towels, hot water bags, and hot patches) lack temperature regulation, which can cause either burn hazards or diminishing treatment effectiveness over time. Some commercial heating wraps and medical devices can control and maintain the heating temperatures, while they are often bulky and heavy to wear continuously. Additionally, joints of arthritis patients are adversely affected by cold and humid environments before the awareness of patients, while existing thermotherapy methods are passive and do not have automatic sensing functions, thus they usually fail to assess when treatment is needed. As a result, there is an urgent need for a timely, automated, safe, stable, and portable thermotherapy solution for arthritis patients.

Recently, due to the innovations in flexible electronics, significant advancements have been made in wearable devices for personal thermal management and healthcare. Flexible Joule heaters that offer on-demand temperature control by adjusting the applied voltage have been developed. For example, Gong et al.¹² reported a thermoresponsive polymer nanomesh film that can function as a flexible Joule heater, triggering the on-demand release of

Correspondence: Mengxi Wu (mengxiwu@dlut.edu.cn) or Junshan Liu (liujsh@dlut.edu.cn)

¹State Key Laboratory of High-performance Precision Manufacturing, Dalian University of Technology, 116024 Dalian, Liaoning, China

²Key Laboratory for Micro/Nano Technology and System of Liaoning Province, Dalian University of Technology, 116024 Dalian, Liaoning, China
Full list of author information is available at the end of the article

© The Author(s) 2025



Open Access This article is licensed under a Creative Commons Attribution-NonCommercial-NoDerivatives 4.0 International License, which permits any non-commercial use, sharing, distribution and reproduction in any medium or format, as long as you give appropriate credit to the original author(s) and the source, provide a link to the Creative Commons licence, and indicate if you modified the licensed material. You do not have permission under this licence to share adapted material derived from this article or parts of it. The images or other third party material in this article are included in the article's Creative Commons licence, unless indicated otherwise in a credit line to the material. If material is not included in the article's Creative Commons licence and your intended use is not permitted by statutory regulation or exceeds the permitted use, you will need to obtain permission directly from the copyright holder. To view a copy of this licence, visit <http://creativecommons.org/licenses/by-nc-nd/4.0/>.

antibiotics to combat bacterial infection at wound sites. Zhao et al.¹³ developed a multifunctional MXene-based smart fabric for biomedical applications, incorporating a safe, all-in-one thermotherapy platform with a humidity-dependent temperature response mechanism. Materials used in Joule heaters, including metals, are also suitable for resistance temperature detection. However, to achieve safe and intelligent on-body heating, an independent temperature sensor for real-time feedback is necessary. To gain the ability of feedback control, Ge et al.¹⁴ developed a smart dressing for exudate managing and on-demand treatment of chronic wounds, which utilizes a liquid metal Joule heater and a commercial temperature & humidity sensor (SHT21, Sensirion, Switzerland). Park et al.¹⁵ presented a skin-integrated system with programmable thermal interface, featuring a fractal-shaped Cu electrode as a heating element and an NTC thermistor (ERT-J0EV104FM, Panasonic, Japan). However, the device has a rigid encapsulation that can impair sensor response performance and cause modulus mismatch with flexible electronics. To solve this issue, researchers integrated self-developed thin-film temperature sensors with heaters. Kang et al.¹⁶ presented a multifunctional, wearable thermal patch composed of a graphene-based Joule heater as well as a capacitive temperature sensor array for thermotherapy. Liu et al.¹⁷ proposed an all-in-one self-degradable flexible skin patch, which consists of a Zn-Ag grid-line Joule heater and a Zn temperature sensor. These devices demonstrate the function of accelerating wound healing by animal experiments, however, they are not suitable as a wearable thermal treatment device for arthritis patients due to three shortcomings. First, the devices are not stretchable, thus they are hard to adapt to the movements of joints, which are the typical lesions of arthritis. Second, the devices do not have the function to sense humidity, which is another major cause of arthritis. At last, the heater is installed under the temperature sensor, which may cause the failure of the temperature sensor regarding heating temperature feedback before human skin gets burned.

In this work, we present a stretchable multifunctional wearable system that can perform real-time monitoring of the joint's microenvironment and conduct on-demand thermotherapy automatically. The system integrates a thin-film Au temperature sensor, a poly(3,4-ethylenedioxythiophene) (PEDOT) humidity sensor, and an Au heater, stacked layer by layer on a kirigami–serpentine polyimide (PI) substrate. The kirigami–serpentine structure enables the stretchability of the device as well as rapid response of sensing and heating. Also, all the layers have a homomorphic shape, offering easy de-coupling of dual-modal sensing signals. The system utilizes a flexible printed circuit for real-time signal processing, close-loop control, and wireless transmission, and a rechargeable soft

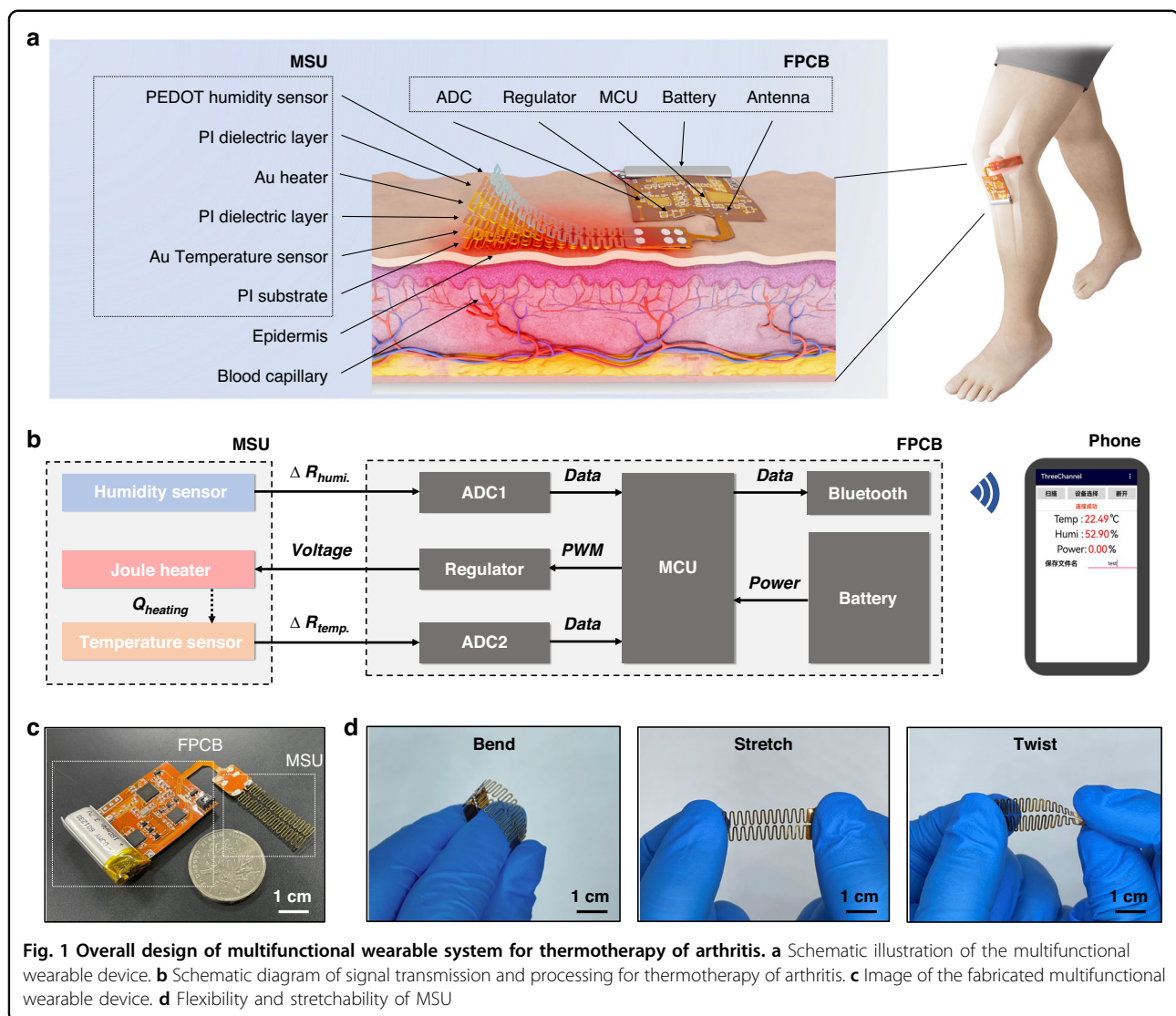
pack battery for power supply. The performance of the sensors and heater is characterized, verifying their fast response and good stability. Based on the real-time monitoring and feedback function of our system, we demonstrate three applications, including programmable on-demand thermotherapy, real-time personal thermal management and thermal dehumidification, covering personal treatment to daily management. Furthermore, the effect of thermotherapy empowered by our system is evaluated by photoplethysmography (PPG) technique. Our work enables a series of user-friendly wearable and wireless gears that can significantly promote the effectiveness and convenience of arthritis management, and therefore is able to relieve the pain of numerous patients.

Results and discussion

Design of the system

Figure 1a illustrates the overall design of the multifunctional wearable arthritis thermotherapy system. The device mainly consists of two parts: a multilayered serpentine-shaped unit (MSU) and a flexible printed circuit board (FPCB). The MSU (4 cm × 1 cm in area) integrates an Au temperature sensor, an Au heater, and a PEDOT humidity sensor on a kirigami–serpentine polyimide (PI) substrate layer by layer. Au is selected for the material of the temperature sensor and the Joule heater due to its excellent stability, ductility, conductivity, and high temperature coefficient of resistance (TCR)¹⁸. PEDOT is chosen as the material of the humidity sensor because of its high conductivity and humidity sensitivity¹⁹. Most commercial PEDOT is doped with polystyrene sulfonate (PSS) to enhance its water solubility; however, the non-conductive PSS groups can reduce conductivity²⁰. To solve this issue, a secondary doping is performed to the PEDOT:PSS solution to improve its stretchability and conductivity^{21,22}. The control of arthritis thermotherapy and signal processing & transmission functions are done by an FPCB, with schematic diagram shown in Fig. 1b. The FPCB (4 cm × 5 cm in area without extended pads) primarily contains two analog-to-digital converter (ADC) chips, a microcontroller unit (MCU) chip, a Bluetooth low energy (BLE) chip, and several RCL components for signal acquisition, processing, and wireless transmission. The entire system is powered by a rechargeable soft pack battery. The MSU and FPCB pads are connected using conductive silver paste. The alignment of two components is achieved with the assistance of through-hole solder pads on the FPCB, which can constrain the uncured conductive silver paste to only cover the pad area of the MSU (Fig. 1c). The details of the fabrication process can be found in the Methods section and Supplemental Material (Fig. S1).

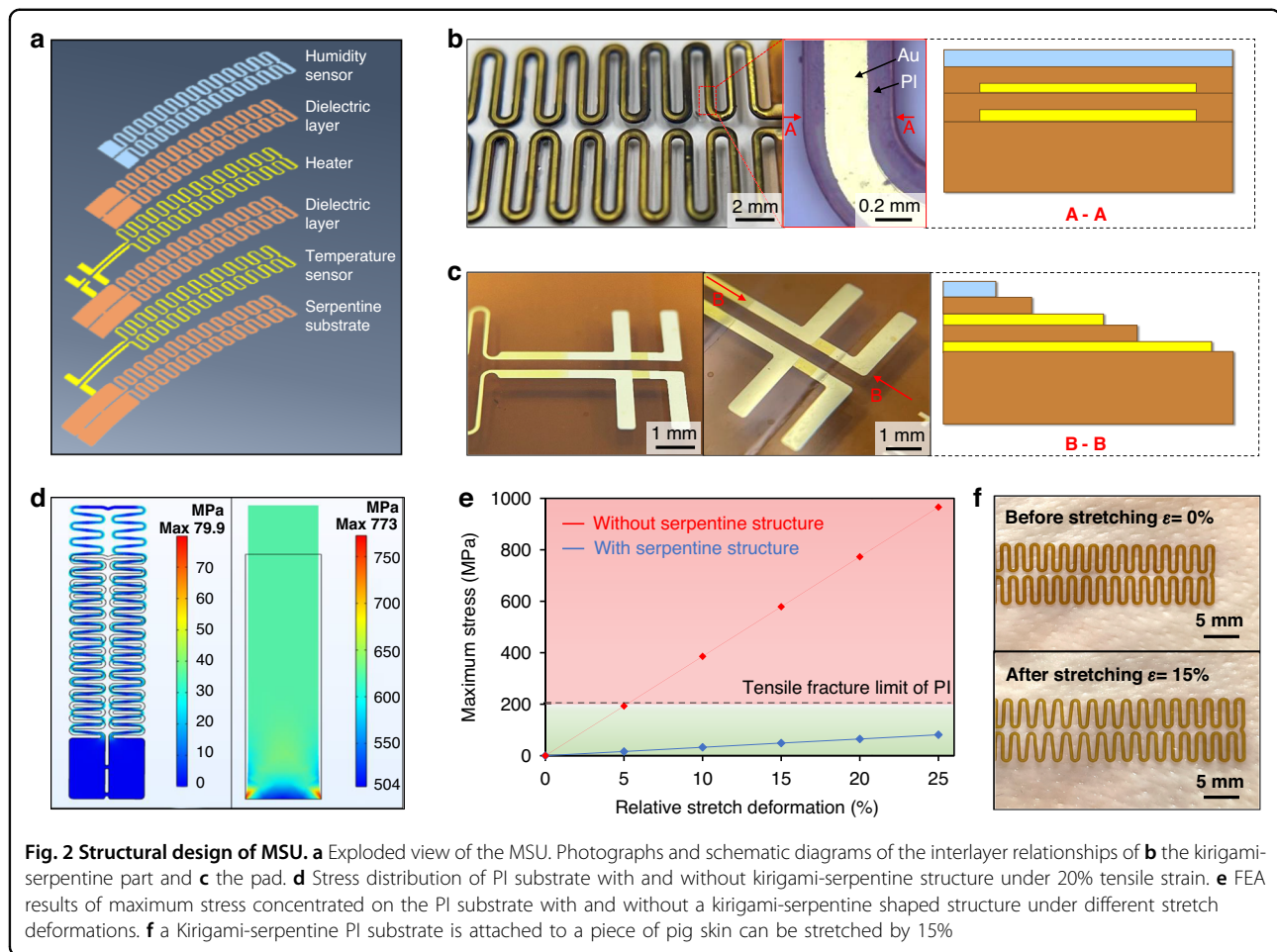
It is well known that PI film is suitable to serve as the substrate or insulation layer of flexible electronics for its



excellent thermal stability, chemical durability, electrical insulation and mechanical property^{23–26}. However, PI has relative limited stretchability comparing with other commonly used flexible substrate materials (such as TPU^{27–29}, PDMS^{30–32}, Ecoflex^{33–35} and hydrogel^{36–38}). To accommodate deformation induced by wearing or the movement of joints, the PI substrate of the MSU is designed as a hollowed kirigami-serpentine shape to enhance its stretchability (Fig. 1d). The designed structure can be reversibly stretched easily, reducing the maximum stress by converting the tensile strain to bending deformation.

The detailed design of MSU is shown in Fig. 2. The temperature sensor, humidity sensor and Joule heater have homomorphic kirigami-serpentine structure. Two PI dielectric layers for insulation are sandwiched between the substrate and the functional layers (Fig. 2a). As shown in Fig. 2b, the functional components of the sensors and the

heater share the same shape as the serpentine PI substrate, while the line width of the temperature sensor and heater is slightly narrower than the substrate, ensuring complete insulation after laser cutting of the PI substrate. Furthermore, as depicted in Fig. 2c, the area of the upper layer is smaller than that of the lower layer to locally expose the pads of the sensors and heater. The kirigami-serpentine structure ensures a larger deformation range. Finite element analysis (FEA) was conducted using COMSOL Multiphysics software to illustrate the stress distribution of the PI substrate during stretching deformation (Fig. 2d). According to literature, the tensile strength of PI film is generally below than 200 MPa³⁹. As shown in Fig. 2e, the FEA results indicate that the maximum stress of a PI film without a serpentine structure exceeds the tensile fracture limit when stretching deformation is 5%. In contrast, the kirigami-serpentine



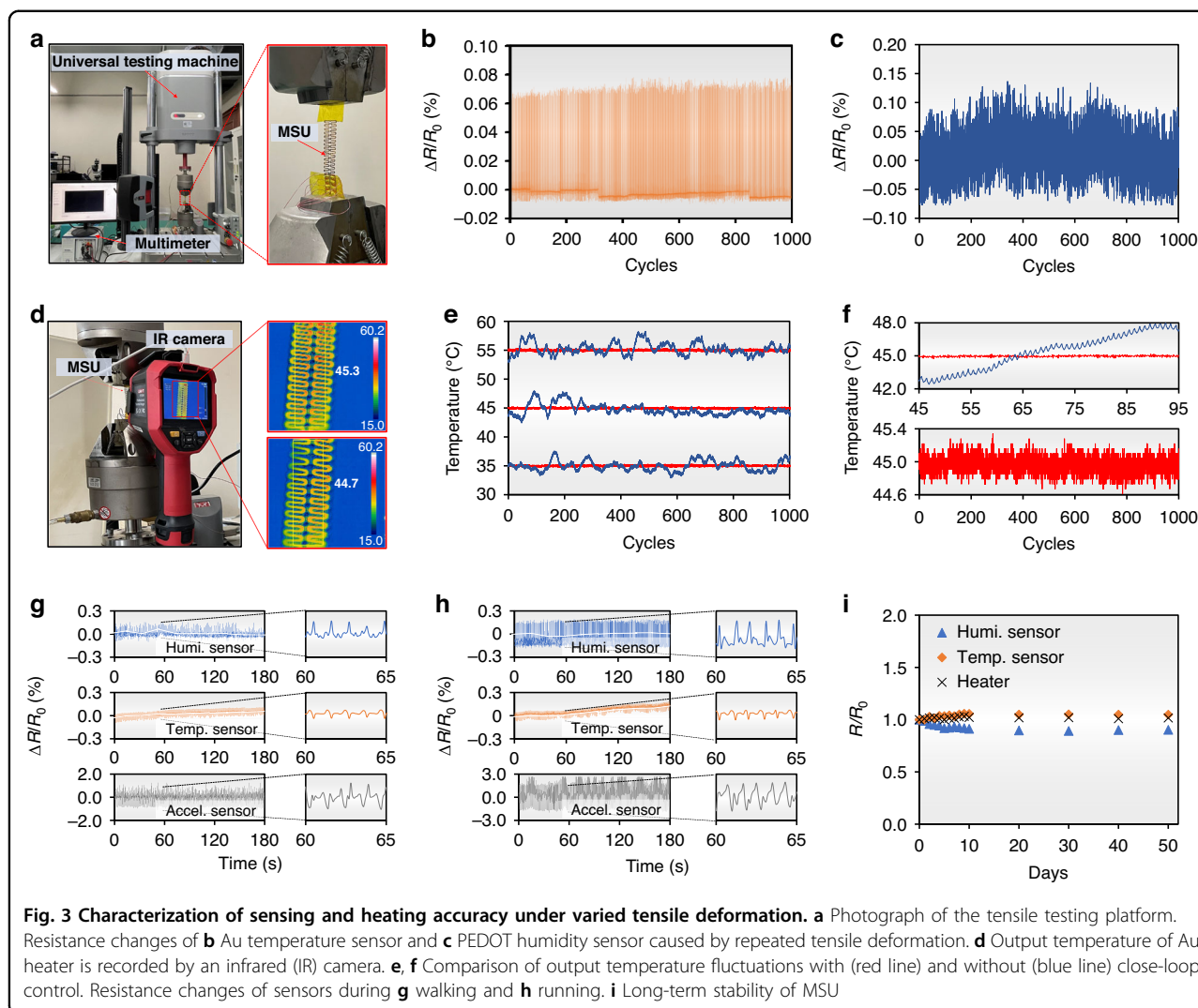
structure can withstand over 25% tensile deformation with stress smaller than 100 MPa, just half of the tensile fracture limit. Figure 2f shows the results of the stretching experiments. The hollowed serpentine PI device is attached to skin and stretched for 15% without fracture. According to literature, though at certain position the joint movements can deform the skin by more than 50%, for most parts the deformation is less than 20%^{40–43}. For the selected wearing position in this paper, our experiment data shows the strain on the knee in different directions are less than 20% after bending (Fig. S2). The results verify the kirigami-serpentine shape sensor can sustain strain caused by joint movements.

Characteristics of sensors and heater

The performance of Au temperature sensor, PEDOT humidity sensor and the heater is investigated and presented in Fig. S3. As shown in Fig. S3a, the resistance of the Au temperature sensor exhibits a linear response (linearity = 0.999) to temperature variations from 10 °C to 50 °C, with a TCR of 0.31%/°C, which is comparable to commercial platinum thermistors (0.39%/°C). Benefiting

from the excellent thermal stability and low thermal expansion coefficient of PI, the temperature sensor provides stable responses to constant temperatures at various levels (Fig. S3b). The thin-film and hollowed feature allows the Au temperature sensor to reach thermal equilibrium with the heat source quickly. The response time and recovery time of the Au temperature sensor, defined as the time to reach 90% of the steady-state value, are 0.27 s and 1.58 s, respectively (Fig. S3c). Additionally, due to the encapsulation of the PI dielectric layer, the Au temperature sensor shows almost no response to humidity changes (Fig. S3d).

The PEDOT humidity sensor is sensitive to both temperature and humidity variations. Here, the sensitivity of the humidity sensor is defined as $S = \frac{\Delta R}{R_0} / \Delta \%RH$. As shown in Fig. S3d, the PEDOT layer exhibits a segmented linear response to humidity changes, with a sensitivity of -0.086 in the range of 10% RH to 45% RH, and -0.034 in the range of 45% RH to 90% RH. Meanwhile, the resistance of the PEDOT humidity sensor also shows a linear response (linearity = 0.997) to temperature, with a TCR of $-0.41\%/^{\circ}\text{C}$ (Fig. S3a), which simplifies the decoupling of



temperature-induced crosstalk in the PEDOT humidity sensor. The PEDOT humidity sensor shows stable responses to constant humidity at different levels (Fig. S3e), with a response time and recovery time of 0.02 s and 15.76 s, respectively (Fig. S3f).

As illustrated in Fig. S3g, the output temperature of Au heater is increased with applied voltage, which matches with Joule's law. This relationship can be used to realize the desired temperature by adjusting the applied voltage, but it also induces a delay of several minutes for heating. Moreover, it is hard to guarantee the safety of the heating process without real-time feedback of heating temperature. Herein, the Au heater and Au temperature sensor are simultaneously controlled by the MCU. A pulse-width modulation (PWM) based on proportional integral derivative (PID) control is applied to realize an accurate, stable and rapid close-loop control of heating process (as shown in Fig. S3h). According to the results in Fig. S3i, it takes less than a second for Au heater to heat up from the

room temperature ($\sim 25^{\circ}\text{C}$) to 45°C , which is obviously faster than the heater without close-up control in Fig. S3g, and faster than other reported studies (Table S1)^{12–17,42–55}.

Tensile test

The signal accuracy of resistive-type sensors is usually compromised by repeated use and deformation, particularly by tensile strain. The preferred strategies to suppress such impacts include de-coupling the signals with the help of an additional strain sensor^{26,56}, using intrinsically strain-insensitive materials^{57,58}, or deformation-insensitive geometric designs^{59–61}. Here, we verified that the kirigami-serpentine structure can mitigate the effects of tensile strain, resulting in negligible disturbances to the sensor resistance.

As shown in Fig. 3a–c, when the MSU is repeatedly stretched from 0 to 20%, the maximum relative changes in resistance of the Au temperature sensor and PEDOT humidity sensor are 0.08% and 0.14%, respectively,

corresponding to measurement errors of 0.26°C and -4.11% RH, which meet the B-class accuracy specified by the international standard IEC 60751-2022. Besides sensing, the stability of heating temperature is crucial not only for the effectiveness but also for the safety of thermotherapy treatment. As shown in Fig. 3d, the output temperature of the Au heater during repeated tensile deformation is recorded by an infrared camera. During the stretching process, fluctuations in the output temperature of the Au heater are primarily caused by two factors: noticeable while irregular fluctuations caused by environmental disturbances (Fig. 3e), and relatively small while regular variations due to stretching deformation (Fig. 3f). In contrast, due to the high accuracy and instant feedback provided by the Au temperature sensor, the Au heater with closed-loop control is able to consistently and rapidly maintain a stable output at different target temperatures over 1000 cycles (Fig. 3f). For example, for the preferred thermotherapy temperature of 45°C , the maximum deviation in output temperature of the heater with and without closed-loop control are -0.39°C to 0.34°C and -2.59°C to 2.97°C , respectively. These results demonstrate that closed-loop control can effectively suppress output temperature fluctuations of the Au heater by an order of magnitude compared to the heater without closed-loop control. Additionally, by using the serpentine structure to counteract the effects of tensile strain, the average heating temperature with closed-loop control is $44.96 \pm 0.09^{\circ}\text{C}$ (Fig. 3f). This indicates that our system can reduce the deviation in heating temperature to less than 0.1°C at 45°C , ensuring the stability and safety of thermotherapy treatment.

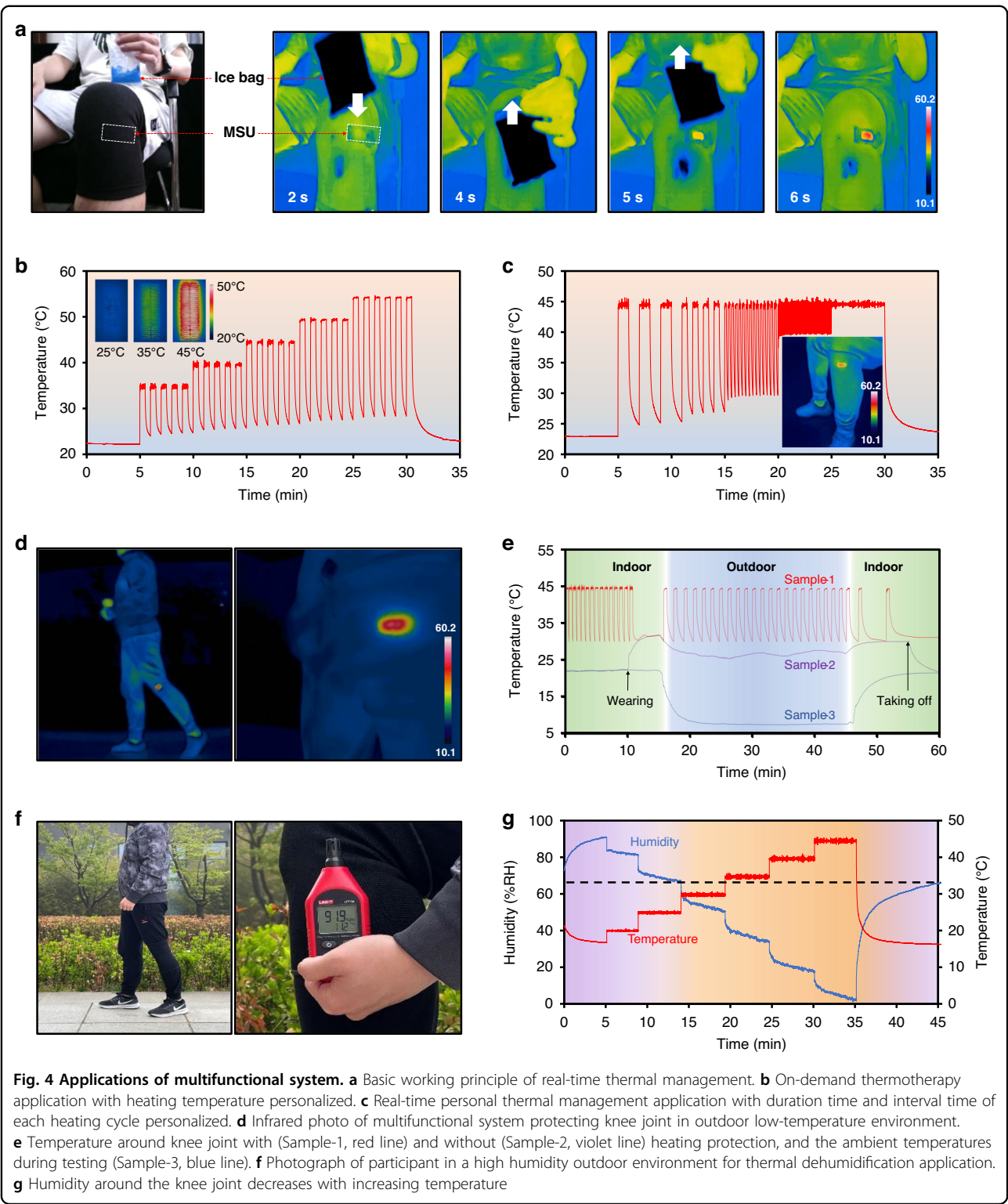
In addition, the influence of human motion on our system was investigated. Figure 3g, h demonstrates the relative resistance change of the temperature sensor and humidity sensor during walking (the speed is $\sim 3\text{ km/h}$) and running (the speed is $\sim 7\text{ km/h}$), respectively. The system was fixed on the joint of the participants by transparent medical tape (Fig. S4), and an accelerometer (MPU6050, TDK InvenSense, USA) was integrated onto the FPCB to monitor the movement of knee joints. It is noted that periodic fluctuations are recorded by the humidity and temperature sensors. The fluctuations match the signals recorded by the accelerometer, which reflects the step frequency of walking or running. Although the motion of humans can induce notable fluctuations in the sensors, the accurate humidity and temperature can be obtained by calculating the average as indicated by the dashed lines in Fig. 3g, h. The humidity is almost constant when the participant is walking, while it shows a slight increase when running. On the other hand, the temperature increases 0.34°C and 0.59°C when walking and running, respectively. Considering the temperature rise and sweating caused

by exercise, the on-body test results are reasonable. Furthermore, to evaluate the long-term stability of our stretchable device, the electrical resistance of MSU was recorded after daily testing. As shown in Fig. 3i, the electrical resistance of both sensors and the heater remains nearly constant during the test. The consistency results are comparable to the studies reported in other literatures^{44,47,53}.

On-body applications

The multifunctional system is compact and lightweight (Fig. S5) to be easily integrated into clothing for wearable real-time thermotherapy and thermal management. For demonstration, the multifunctional system was attached to a knee (Figure S6). The basic working principle of a multifunctional system for knee joint protection is illustrated in Fig. 4a. When a cold source (ice pack) approaches the knee joint and brings the temperature down to an unhealthy level, the heater rapidly responds and warms up until the temperature of knee joint returns to normal. Based on this fundamental principle, three extended applications are demonstrated in Fig. 4b–g. The first one is programmable on-demand thermotherapy. As shown in Fig. 4b, c, the temperature, duration, and interval time of each heating cycle can be customized according to medical advice. The programmable multifunctional system enables arthritis patients to receive personalized thermotherapy regardless of time and place limitations.

The second application is real-time personal thermal management. For arthritis patients, it is crucial to focus not only on regular treatment but also on daily management. As shown in Fig. 4d, the multifunctional system was mounted on the knee joint of the participant and collected data during the process of wearing, walking and taking off. Figure 4e displays the process of the system maintaining the temperature around the knee joint from indoor to outdoor and then back indoor (Sample-1). For comparison, two other devices were used to record temperature variations of the knee joint without heating (Sample-2) and the environment temperature (Sample-3). The preset threshold temperature to trigger heating is 30°C , and the target heating temperature is 45°C . At the beginning of the test (0th min to 10th min in Fig. 4e), the multifunctional system senses the room temperature indoor is $\sim 22^{\circ}\text{C}$, thus the heater raises the temperature to the target level (45°C) for preheating before wearing. When the volunteer stays indoors, the temperature of the knee joint can be maintained, so the heater stops heating to conserve power (10th min to 15th min in Fig. 4e). While when the volunteer is moving to an outdoor environment (15th min to 45th min in Fig. 4e), the cold environment ($\sim 7^{\circ}\text{C}$) rapidly drops the temperature of the knee joint to lower than the preset minimum temperature, prompting



the heater to respond quickly and raise the temperature again to keep the knee warm. After returning indoors (45th min to 60th min in Fig. 4e), the heater continues running to accelerate the temperature of knee recovery.

The third application is thermal dehumidification. In addition to cold environments, damp air is also detrimental to arthritis patients. The degree of humidity in the air is typically evaluated by relative humidity, which is the

ratio of the actual water vapor pressure to the saturated water vapor pressure. As demonstrated in Fig. 4f, when the participant wears our device and enters a high humidity environment (over 90% RH), the heater activates. As the temperature rises, the saturated water vapor pressure increases sharply, leading to a rapid drop in relative humidity during the heating period (5th min to 35th min in Fig. 4g). Simultaneously, heating promotes the evaporation of moisture from the clothing and disperses the water vapor in the microenvironment around the knee joint. Compared to the initial conditions, this change results in a significant decrease in the actual water vapor pressure. Therefore, the control of relative humidity can still be maintained for a period of time, even after heating (35th min to 45th min in Fig. 4g).

Evaluation of thermotherapy effect by PPG

Appropriate thermal therapy can facilitate local vasodilation and enhance blood perfusion⁶² to eliminate inflammatory substances¹¹, thereby alleviating swelling, relieving pain, and inhibiting the progression of arthritis. Here, in order to verify the effect of our wearable system, the PPG technique was employed to measure blood perfusion in local microcirculation. A standard PPG module consists of a light-emitting diode (LED) that emits light and a photodetector that detects the emitted light⁶³. The basic principle of the reflective-type PPG module is illustrated in Fig. 5a. When the light emitted by the LED passes through the human body, it is partially absorbed. The remaining reflected and scattered light is detected by the photodetector and converted into an electrical signal, i.e., the PPG signal. As shown in Fig. 5b, the waveform of PPG signals can be divided into pulsatile part and steady part. The pulsatile part is related to the volume change of blood in the arteries, originating from the cardiac cycle. The steady part, or non-pulsatile part, is influenced by biological characteristics such as skin color, tissue composition, and ambient light. Since the blood absorbs more light than surrounding tissues, an increase in blood flow will lead to a more pronounced changes in the pulsatile part of PPG signals.

As shown in Fig. 5c, the MSU and PPG module are securely attached to the knee joint using a light-proof medical tape to measure changes in the PPG signal in situ. The volunteer maintains a fixed sitting position during signal acquisition to minimize interference from motion artifacts. Figure 5d illustrates the PPG signal before, during, and after the heating process of thermotherapy. Compared to the signal before heating (insert figure (i) of Fig. 5d), the increased blood flow results in a noticeable increase in the amplitude of the pulsatile part of the PPG signal (insert figure (ii) of Fig. 5d). When the heating stops, the PPG signal returns to its pre-heating level (insert figure (iii) of Fig. 5d). In addition, the PPG signals from the other eight samples are recorded in Fig. 5e and Figure S7. The

selected volunteers are healthy adults with normal blood circulation function, including four males and four females, with age ranging from 23 to 30. The heating starts from the 5th min and ends at the 10th min with the temperature set at 45 °C. For all eight samples, a significant increase in the amplitude of the pulsatile part of the PPG signal can be found after applying thermotherapy, as shown in Fig. S8. The amplitude of the pulsatile part (calculated as average relative amplitude change) increases from 1.0‰ to 2.5‰, with an increase of $149.5 \pm 61.5\%$. The reproducible and distinguishable trend indicates that PPG signal can be used to reflect the dilation of local blood vessels under thermal stimulation. Although the specific relationship between thermotherapy parameters and treatment efficacy remains to be explored, it has been confirmed that such-like devices can improve blood flow at the joint^{44,47} and relieve pain during the clinical trial⁹. The results demonstrate our system offers a convenient and effective method for patients with arthritis to perform thermotherapy on-demand.

Conclusions

In summary, we designed and fabricated a wearable electronic system for smart and real-time thermotherapy of arthritic joints. Our device integrates a thin-film Au temperature sensor, Au heater, and PEDOT humidity sensor in a layer-by-layer arrangement on a PI substrate with a kirigami-serpentine structure. This multilayer stacked configuration leverages the advantages of micro/nanoscale thin-film functional layers, offering higher integration compared to conventional multifunctional devices that place functional units on the same plane. The thin-film feature and closed-loop control enable the Au temperature sensor and heater to respond rapidly, providing timely, safe, and stable thermotherapy for arthritis patients. Furthermore, we demonstrated the application of our device for personal thermotherapy treatment and real-time thermal management. A preliminary analysis was conducted to evaluate the effect of thermotherapy on enhancing blood perfusion using the PPG technique. Our system is validated to be effective to keep the joints warm and low humidity in an automated, rapid, and stable manner. In addition, it provides safe and personalized schemes for arthritis thermotherapy.

Methods

Consent to participate

Informed consent has been obtained from the volunteers who participated in the experiments.

Fabrication process of multilayered serpentine unit

Preparation of PI substrate

First, a 75 µm thick PI film (BL0425, Guangzhou Shibeidragon Electronics, China) was cut into pieces of 70 mm × 23 mm. Then the PI film was sequentially ultrasonically

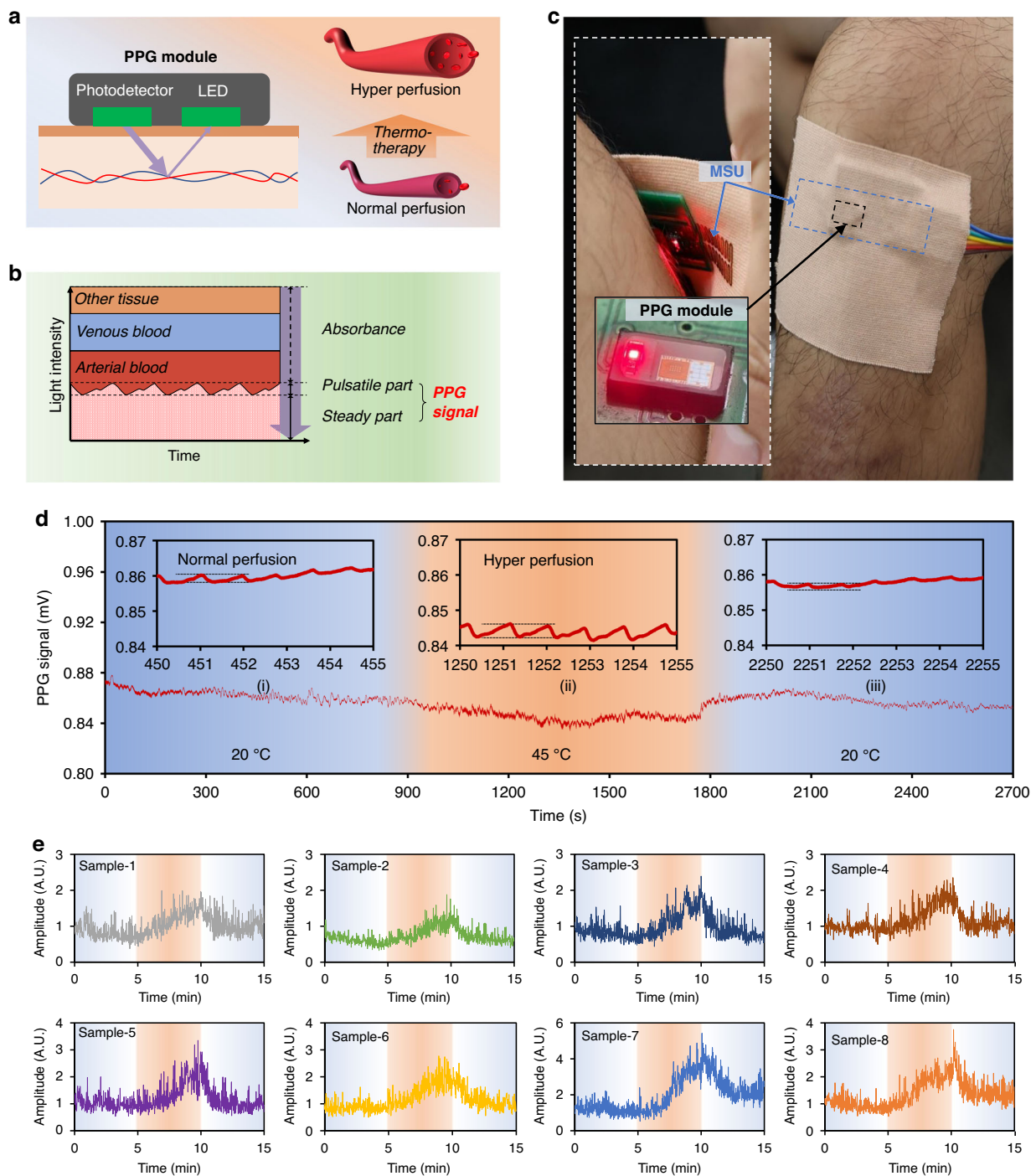


Fig. 5 Characterization of blood perfusion because of thermotherapy. **a** Schematic diagram of the relationship between vascular dilation and PPG signal. **b** Composition of PPG signal. **c** Experimental setups for PPG signal acquisition during thermotherapy offered by the multifunctional system. **d** PPG signal before (0~900 s), during (900~1800 s), and after (1800~2700 s) thermotherapy. The higher variation amplitude of PPG signal during thermotherapy (insert figure ii) than before (i) or after (iii) thermotherapy indicates that hyper perfusion of blood vessels occurs. **e** Amplitude variations of PPG signals recorded from 8 participants all present notable increase during thermotherapy (time interval from 5th to 10th min)

cleaned in acetone and ethanol for 30 min and then rinsed by deionized water. After blowing by nitrogen gas and drying on an 85 °C hot plate for 30 min, the clean PI film

was flat fixed on a 76 mm × 23 mm glass sheet by 3 mm PI tape (Kapton, DuPont, USA), as the substrate of a multilayered serpentine unit.

Fabrication of Au temperature sensor

First, a 100 nm thick Au film was deposited on PI substrate by magnetron sputtering (Lab 18, Kurt J. Lesker, USA). Then, a positive photoresist (AZ MIR 703, AZ Electronic Materials, USA) film was spin-coated at 600 rpm for 9 s and 2500 rpm for 30 s, and soft baked on an 85 °C hot plate for 30 min. As follow, the photoresist layer was exposed for 350 mJ/cm² (MA/BA6, SUSS Micro Tec, Germany) after covering with a film mask (Shenzhen Qingyi Photomask, China), and patterned by developer (AZ 400 K, AZ Electronic Materials, USA) to serve as the mask of wet etch of Au film. Subsequently, the Au film was immersed in a mixture of KI, I₂, and H₂O (10 g: 2 g: 100 mL) for 20 s to remove the part without protection of the patterned photoresist mask. Finally, the photoresist layer was flood-exposed for 350 mJ/cm² and then removed by developer.

Fabrication of PI dielectric layer

First, a wafer protective film with weak adhesion was covered on the pad area of the Au temperature sensor. Then, the precursor of PI (PAA-1003, Changzhou Yaan New Materials, China) was spin-coated on the PI substrate at 600 rpm for 9 s and 4000 rpm for 30 s, to cover the Au temperature sensor. After that, the wafer protective film was peeled off to partly expose the pad area. Finally, the precursor was step-baked and imidized in the oven at 80 °C, 160 °C, and 220 °C for 10 min sequentially to cure as PI dielectric layer. In addition, another PI dielectric layer was formed using the same process after the fabrication of the Au heater.

Fabrication of an Au heater

First, a 400 nm thick Au film was deposited on PI substrate by magnetron sputtering. Then, the Au was patterned by the same process in the fabrication of the Au temperature sensor.

Fabrication of PEDOT humidity sensor

First, a wafer protective film with weak adhesion was covered on the pad area of the Au temperature sensor and Au heater. Then, a PEDOT:PSS solution (Meryer (Shanghai) Biochemical Technology, China) was doped with dimethyl sulfoxide (Meryer (Shanghai) Biochemical Technology, China) and triton X-100 (Meryer (Shanghai) Biochemical Technology, China) at a weight ratio of 50: 2: 1. Finally, the mixture was spin-coated on PI substrate at 600 rpm for 9 s and 3000 rpm for 30 s, and cured on 85 °C hot plate for 30 min.

Laser cutting of kirigami-serpentine shape

After all function layers were integrated, the PI substrate was cut by a femtosecond laser, with a power of 30 W and a pulse width less than 300 fs, to preserve the serpentine structure.

Characterization of temperature and humidity sensor

The relationship curve of sensors was investigated in a temperature and humidity controllable chamber (JK-HW-50L, Pinsheng, China), the humidity was maintained at 50% RH during the temperature test in Fig. S3a, b, and the temperature was maintained at 20 °C during the humidity test in Fig. S3d, e. The MSU was placed out of the chamber during the response test in Fig. S3c, f, the response and recovery time of sensors were evaluated by using an air flow exported from the chamber to brush the MSU. During the temperature response test in Fig. S3c, the temperature and humidity of air flow were 45 °C and 50% RH (same as the room humidity), respectively. During the humidity response test in Fig. S3f, the temperature and humidity of the air flow were the same as the room temperature (20 °C) and 90% RH, respectively. The strain during the tensile test was applied by a universal testing machine (E3000, Instron, USA). The resistance of sensors was collected by an eight-channel digital multimeter (TRION-2402-MULT-8-L0B, Dewetron, Austria) during the aforementioned tests.

Characterization of heater

The Joule heating performance of the Au heater was investigated by a digital thermometer (TX1002, Yokogawa, Japan) and powered by a constant voltage source (N2600-020-01, Hunan Next Generation Instrumental, China), the room temperature was maintained at 20 °C during the tests.

Tensile test

The MSU was stretched by the universal testing machine (E3000, Instron, USA). The resistance variation of Au temperature sensor and PEDOT humidity sensor was recorded by a digital multimeter (PXIe-4081, National Instruments, USA), and the heating temperature of Au heater was recorded by an infrared camera (UTI320E, UNI-Trend technology, China). The frequency of tensile cycles was 1 Hz. During the tensile test, the room temperature and humidity were maintained at 20 °C and 50% RH, respectively.

Characterization of PPG signal

The PPG module (MAX30102, Maximintergrated, USA) was driven by a minimum system board (STM32f103c8t6, STMicroelectronics, TNCs). The sampling frequency of the PPG signal was 100 Hz. The room temperature was maintained at 20 °C during the tests.

Acknowledgements

This work was supported by the National Natural Science Foundation of China (U23A20362, 51875083), and the funding from Dalian University of Technology (DUT23YG215, DUT22LAB504).

Author details

¹State Key Laboratory of High-performance Precision Manufacturing, Dalian University of Technology, 116024 Dalian, Liaoning, China. ²Key Laboratory for Micro/Nano Technology and System of Liaoning Province, Dalian University of Technology, 116024 Dalian, Liaoning, China. ³State Key Laboratory of Digital Manufacturing Equipment and Technology, Huazhong University of Science and Technology, 430074 Wuhan, China. ⁴National Key Laboratory of Science and Technology on Micro and Nano Fabrication School of Electronic Information and Electrical Engineering, Shanghai Jiao Tong University, 200240 Shanghai, China. ⁵Institute of Flexible Electronics, Northwestern Polytechnical University, 710072 Xi'an, China

Author contributions

Z. L., X. W., Y. H. and W. H. designed, fabricated, and characterized the devices. Z. L., P. S., W. L. and Y. H. designed and fabricated the signal acquisition, processing, and transmission circuits. Z. L., P. S. and Y. H. analyzed data and prepared figures. Z. L., M. W. and J. L. wrote the manuscript. M. W., L. W. and J. L. supervised this project.

Data availability

The data is available from the corresponding authors upon reasonable requests.

Conflict of interest

The authors declare no competing interests.

Supplementary information The online version contains supplementary material available at <https://doi.org/10.1038/s41378-025-00912-8>.

Received: 14 November 2024 Revised: 17 February 2025 Accepted: 24 February 2025

Published online: 13 May 2025

References

- Loeser, R. F., Goldring, S. R., Scanzello, C. R. & Goldring, M. B. Osteoarthritis: A disease of the joint as an organ. *Arthritis Rheum* **64**, 1697–1707 (2012).
- Smolen, J. S. & Aletaha, D. Rheumatoid arthritis therapy reappraisal: strategies, opportunities and challenges. *Nat Rev Rheumatol* **11**, 276–289 (2015).
- Woo, P. & Wedderburn, L. R. Juvenile chronic arthritis. *Lancet* **351**, 969–973 (1998).
- David, T. F. et al. The prevalence of knee osteoarthritis in the elderly. The Framingham osteoarthritis study. *Arthritis Rheum* **30**, 914–918 (1987).
- Brophy, R. H. & Fillingim, Y. A. AAOS Clinical Practice Guideline Summary: Management of Osteoarthritis of the Knee (Nonarthroplasty), Third Edition. *J Am Acad Orthop Surg* **30**, e721–e729 (2022).
- Knoop, J. et al. Stratified exercise therapy compared with usual care by physical therapists in patients with knee osteoarthritis: a randomized controlled trial protocol (Octopus Study). *Physiother Res Int* **25**, e1819 (2020).
- Branco, M. et al. Bath thermal waters in the treatment of knee osteoarthritis: a randomized controlled clinical trial. *Eur J Phys Rehabil Med* **52**, 422–430 (2016).
- Fransen, M., Crosbie, J. & Edmonds, J. Physical therapy is effective for patients with osteoarthritis of the knee: a randomized controlled clinical trial. *J Rheumatol* **28**, 156–164 (2001).
- Michlovitz, S., Hun, L., Erasala, G. N., Hengehold, D. A. & Weingand, K. W. Continuous low-level heat wrap therapy is effective for treating wrist pain. *Arch Phys Med Rehabil* **85**, 1409–1416 (2004).
- Petrofsky, J. S., Laymon, M. & Lee, H. Effect of heat and cold on tendon flexibility and force to flex the human knee. *Med Sci Monit* **19**, 661–667 (2013).
- Shang, H., Gu, H. & Zhang, N. From traditional to novel treatment of arthritis: a review of recent advances in nanotechnology-based thermal therapy. *Nanomedicine* **16**, 2117–2132 (2021).
- Gong, M. et al. Flexible breathable nanomesh electronic devices for on-demand therapy. *Adv Funct Mater* **29**, 1902127 (2019).
- Zhao, X. et al. Smart Ti₃C₂T_x MXene fabric with fast humidity response and joule heating for healthcare and medical therapy applications. *ACS Nano* **14**, 8793–8805 (2020).
- Ge, Z. Y. et al. Wireless and closed-loop smart dressing for exudate management and on-demand treatment of chronic wounds. *Adv Mater* **35**, 2304005 (2023).
- Park, M. et al. Skin-integrated systems for power efficient, programmable thermal sensations across large body areas. *Proc Natl Acad Sci USA* **120**, e2077139176 (2023).
- Kang, M. et al. Wireless graphene-based thermal patch for obtaining temperature distribution and performing thermography. *Sci Adv* **8**, m6693 (2022).
- Liu, J. et al. An all-in-one self-degradable flexible skin patch with thermostatic control and spontaneous release of antibacterial ions to accelerate wound healing. *Adv Mater Technol* **8**, 2202159 (2023).
- Scott, E. A., Carow, A., Pete, D. & Harris, C. T. Comparative analysis of the sensitivity of nanometallic thin film thermometers. *Nanotechnology* **33**, 375503 (2022).
- Daoud, W. A., Xin, J. H. & Szeto, Y. S. Polyethylenedioxythiophene coatings for humidity, temperature and strain sensing polyamide fibers. *Sens Actuators B: Chem* **109**, 329–333 (2005).
- Rahimzadeh, Z., Naghib, S. M., Zare, Y. & Rhee, K. Y. An overview on the synthesis and recent applications of conducting Poly(3,4-Ethylenedioxythiophene) (PEDOT) in industry and biomedicine. *J Mater Sci* **55**, 7575–7611 (2020).
- Oh, J. Y. et al. Effect of PEDOT nanofibril networks on the conductivity, flexibility, and coatability of PEDOT:PSS films. *ACS Appl Mater Interfaces* **6**, 6954–6961 (2014).
- Lipomi, D. J. et al. Electronic properties of transparent conductive films of PEDOT:PSS on stretchable substrates. *Chem Mat* **24**, 373–382 (2012).
- Yang, Y. et al. A laser-engraved wearable sensor for sensitive detection of uric acid and tyrosine in sweat. *Nat Biotechnol* **38**, 217–224 (2020).
- Wang, M. et al. A wearable electrochemical biosensor for the monitoring of metabolites and nutrients. *Nat Biomed Eng* **6**, 1225–1235 (2022).
- Tu, J. et al. A wireless patch for the monitoring of C-reactive protein in sweat. *Nat Biomed Eng* **7**, 1293–1306 (2023).
- Zhang, C. et al. Bioinspired environment-adaptable and ultrasensitive multifunctional electronic skin for human healthcare and robotic sensations. *Small* **19**, e2304004 (2023).
- Li, Y. et al. Continuously prepared highly conductive and stretchable SWNT/MWNT synergistically composited electrospun thermoplastic polyurethane yarns for wearable sensing. *J Mater Chem C* **6**, 2258–2269 (2018).
- Tan, C. et al. A high performance wearable strain sensor with advanced thermal management for motion monitoring. *Nat Commun* **11**, 3530 (2020).
- Zhang, W. et al. Hierarchically interlocked helical conductive yarn enables ultra-stretchable electronics and smart fabrics. *Chem Eng J* **462**, 142279 (2023).
- Yun, T. G. et al. All-transparent stretchable electrochromic supercapacitor wearable patch device. *ACS Nano* **13**, 3141–3150 (2019).
- Yao, S. & Zhu, Y. Wearable multifunctional sensors using printed stretchable conductors made of silver nanowires. *Nanoscale* **6**, 2345–2352 (2014).
- Sarwar, M. S. et al. Bend, stretch, and touch: locating a finger on an actively deformed transparent sensor array. *Sci Adv* **3**, e1602200 (2017).
- Ryu, S. et al. Extremely elastic wearable carbon nanotube fiber strain sensor for monitoring of human motion. *ACS Nano* **9**, 5929–5936 (2015).
- Yeasmin, R., Han, S., Duy, L. T., Ahn, B. & Seo, H. A skin-like self-healing and stretchable substrate for wearable electronics. *Chem Eng J* **455**, 140543 (2023).
- Kim, S. et al. An intrinsically stretchable multi-biochemical sensor for sweat analysis using photo-patternable Ecoflex. *npg Flex Electron* **7**, 33–39 (2023).
- Zhao, Y. et al. Skin-inspired antibacterial conductive hydrogels for epidermal sensors and diabetic foot wound dressings. *Adv Funct Mater* **29**, 1901474 (2019).
- Li, P. et al. Stretchable all-gel-state fiber-shaped supercapacitors enabled by macromolecularly interconnected 3D graphene/nanostructured conductive polymer hydrogels. *Adv Mater* **30**, e1800124 (2018).
- Shen, Z. et al. High-stretchability, ultralow-hysteresis conducting polymer hydrogel strain sensors for soft machines. *Adv Mater* **34**, e2203650 (2022).
- Ma, L., Wang, Y., Wang, Y., Wang, C. & Zhuang, G. Polyimide nanocomposites with reduced graphene oxide for enhanced thermal conductivity and tensile strength. *Mater Res Express* **6**, 125346 (2019).
- Liu, S., Rao, Y., Jang, H., Tan, P. & Lu, N. Strategies for body-conformable electronics. *Matter* **5**, 1104–1136 (2022).
- Hu, X. et al. A super-stretchable and highly sensitive carbon nanotube capacitive strain sensor for wearable applications and soft robotics. *Adv Mater Technol* **7**, 2100769 (2022).

42. Kim, J. et al. Stretchable silicon nanoribbon electronics for skin prosthesis. *Nat Commun* **5**, 5747 (2014).
43. Son, D. et al. Multifunctional wearable devices for diagnosis and therapy of movement disorders. *Nat Nanotechnol* **9**, 397–404 (2014).
44. Choi, S. et al. Stretchable heater using ligand-exchanged silver nanowire nanocomposite for wearable articular thermotherapy. *ACS Nano* **9**, 6626–6633 (2015).
45. Lan, W. et al. Ultraflexible transparent film heater made of Ag nanowire/PVA composite for rapid-response thermotherapy pads. *ACS Appl Mater Interfaces* **9**, 6644–6651 (2017).
46. Ma, Z. et al. High-performance and rapid-response electrical heaters based on ultraflexible, heat-resistant, and mechanically strong aramid nanofiber/Ag nanowire nanocomposite papers. *ACS Nano* **13**, 7578–7590 (2019).
47. Jang, N. et al. Simple approach to high-performance stretchable heaters based on Kirigami patterning of conductive paper for wearable thermotherapy applications. *ACS Appl Mater Interfaces* **9**, 19612–19621 (2017).
48. Li, Y. et al. Multifunctional wearable device based on flexible and conductive Carbon Sponge/Polydimethylsiloxane composite. *ACS Appl Mater Interfaces* **8**, 33189–33196 (2016).
49. Liu, Q. et al. Thermal, waterproof, breathable, and antibacterial cloth with a nanoporous structure. *ACS Appl Mater Interfaces* **10**, 2026–2032 (2018).
50. Yin, M. et al. 3D printed microheater sensor-integrated, drug-encapsulated microneedle patch system for pain management. *Adv Healthc Mater* **8**, 1901170 (2019).
51. Zareei, A. et al. A biodegradable hybrid micro/nano conductive zinc paste for paper-based flexible bioelectronics. *Adv Mater Technol* **7**, 2101722 (2022).
52. Yang, L. et al. Novel gas sensing platform based on a stretchable laser-induced graphene pattern with self-heating capabilities. *J Mater Chem A* **8**, 6487–6500 (2020).
53. Li, Y. et al. A smart, stretchable resistive heater textile. *J Mater Chem C* **5**, 41–46 (2017).
54. Hazarika, A. et al. Woven Kevlar fiber/polydimethylsiloxane/reduced graphene oxide composite-based personal thermal management with freestanding Cu–Ni core–shell nanowires. *Nano Lett* **18**, 6731–6739 (2018).
55. Ma, X. et al. Stretchable and skin-attachable electronic device for remotely controlled wearable cancer therapy. *Adv Sci* **10**, 2205343 (2023).
56. Gong, S. et al. Local Crack-programmed gold nanowire electronic skin tattoos for in-plane multisensor integration. *Adv Mater* **31**, 1903789 (2019).
57. Lee, J. et al. Intrinsically strain-insensitive, hyperelastic temperature-sensing fiber with compressed micro-wrinkles for integrated textronics. *Adv Mater Technol* **5**, 2000073 (2020).
58. Zheng, Z. et al. Strain/deformation-insensitive wearable rubber composite for temperature monitoring based on the photothermal and thermoelectric conversion. *Chem Eng J* **484**, 149329 (2024).
59. Jang, S. et al. A high aspect ratio serpentine structure for use as a strain-insensitive, stretchable transparent conductor. *Small* **14**, 1702818 (2018).
60. Wang, H. et al. Double-sided wearable multifunctional sensing system with anti-interference design for human-ambience interface. *ACS Nano* **16**, 14679–14692 (2022).
61. Yuan, H. et al. Ultra-stable, waterproof and self-healing serpentine stretchable conductors based On WPU sheath-wrapped conductive yarn for stretchable interconnects and wearable heaters. *Chem Eng J* **473**, 145251 (2023).
62. Charkoudian, N. Skin blood flow in adult human thermoregulation: how it works, when it does not, and why. *Mayo Clin Proc* **78**, 603–612 (2003).
63. Park, J., Seok, H. S., Kim, S. & Shin, H. Photoplethysmogram analysis and applications: an integrative review. *Front Physiol* **12**, 808451 (2022).